

Design considerations to fabricate multifunctional superomniphobic surfaces: a review

Jaya Verma^{1*}, Gareth J. Bennett² and Saurav Goel^{1,3*}

¹ School of Engineering, London South Bank University, London, SE1 0 AA, UK

² Department of Mechanical, Manufacturing & Biomedical Engineering, D02 PN40, Trinity College Dublin, Ireland

³ Department of Mechanical Engineering, University of Petroleum and Energy Studies, Dehradun, 248007, India

*Corresponding author: jayaverma745@gmail.com, goels@lsbu.ac.uk

Abstract

A surface possessing repellency to low surface tension liquids e.g., oils and alcohols (superoleophobic) and high surface tension liquids e.g., water (superhydrophobic) is referred to as superomniphobic. Such surfaces are receiving great attention as they can be used in a myriad of industrial and biomedical applications. In this timely review, we discuss the challenges in systematic design and fabrication of superomniphobic surfaces. Particular attention was paid to elucidating the significance of surface energy, roughness and the critical role of re-entrant texture in obtaining the Cassie–Baxter state. We also discussed how hierarchical scales of texture can yield high contact angles and decrease the hysteresis in the contact angle of superomniphobic surfaces by reducing the solid–liquid contact area. On this premise, we discussed design parameters that would allow efficient fabrication of superomniphobic surfaces leading to newer applications and horizons in the field. The review concludes by identifying newer challenges and potential for these surfaces.

1. Introduction

Superomniphobic surfaces can repel various types of liquids and are receiving great attention due to their multifarious use in various applications such as self-cleaning [1, 2], anti-fouling [3, 4], stain-free clothing [5], spill-resistant protective wear [6], drag reduction [7], corrosion prevention [8, 9], microrobot movement [10-12] in aqueous and chemical media and separation of liquids [13-15]. Conventionally, superomniphobic surfaces [16, 17] are largely fabricated through a combination of micro/nano hierarchical structures and subsequent chemical treatments. The range of diverse methods include stacking micro and nanospheres [18, 19], texturing fibers [20], spray coating [15, 21-23] and photolithography [24, 25]. Subsequent chemical treatments are carried out using methods such as dip-coating [19, 20, 22] and vapor

deposition of perfluorocarbon materials onto the hierarchical structured surfaces [24, 25]. The functionality of superomniphobic surfaces is at its best when both structural and chemical properties are preserved.

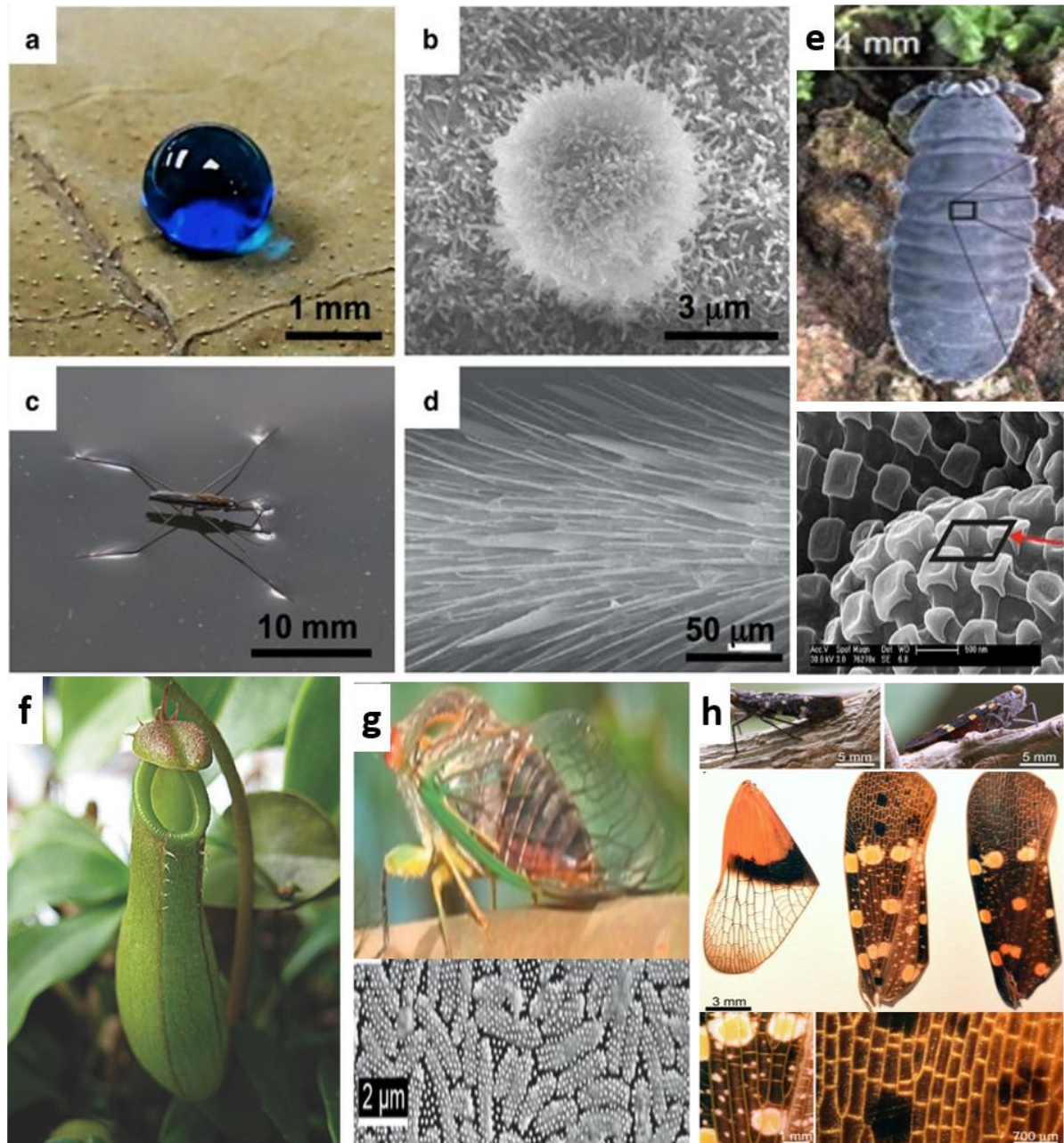


Fig. 1 Naturally occurring super-repellent surfaces. (a) A droplet of water (blue) showing a very high contact angle on a lotus leaf. (b) SEM image of a lotus leaf showing its rough, hierarchical texture. (c) A water strider walking on the water surface. (d) SEM image of a water strider's leg, which consists of numerous oriented hairs. (e) SEM images of hierarchical structured springtails skin where secondary granules (SG) are superimposed on primary granules (SG possess re-entrant texture, which allows springtail skin to be oleophobic) [26] (f) Pitcher plant: Nanostructured surfaces retaining a liquid lubricant, which repels other fluids [27] (g) Anti-fouling inspired by cicadas: (i) The cicada (*P. claripennis*) with (ii) nanofibrils (dots) on the wing surface with attached and killed bacteria (*P. aeruginosa*) [28] (h) Digital photographs of the Australian and Northern Queensland native planthopper, *D. danae*, resting on the branch of the plant *Planchonia careya*., Planthopper hindwing

(left) and forewing (dorsal side; middle image, ventral side image on right), Higher-magnification images of regions on the dorsal section of the forewing showing the pigmentation and vein structure at these scales. [29]

When a surface possesses a contact angle of $> 150^\circ$ and contact angle hysteresis of $< 5^\circ$ for the water droplet, it is regarded as superhydrophobic. Likewise, when a surface possesses a contact angle of $> 150^\circ$ and contact angle hysteresis of $< 5^\circ$ but for low surface tension liquids such as oils, alcohols, or other organic solvents, it is considered as a superoleophobic surface. Superhydrophobic surfaces are pervasive in nature (Fig. 1a–d) and its examples can be seen on plant leaves [26, 30, 31], legs of the water strider [32–34], gecko's feet [3, 4], troughs on the elytra of desert beetles [35] and insect wings [36], possessing extreme water-repellency.

Inspired by natural superhydrophobic surfaces, several researchers have attempted to develop engineered superhydrophobic surfaces [18]. Despite numerous natural superhydrophobic surfaces and rare natural oleophobic surfaces (Fig. 1) [37–40] that are seen in nature, naturally occurring superoleophobic surfaces are not yet reported to date. This is because oils possess significantly lower surface tension than water and can easily spread on the natural surfaces. However, based on previous work [41–51] that recognized the importance of re-entrant texture (Fig. 2e) in designing oil-repellent surfaces, several researchers have now engineered artificial (or synthetic) superoleophobic surfaces [14, 52–54]. Typically, most surfaces that repel lower surface tension liquids, such as oil, can also repel higher surface tension liquids, such as water. Consequently, most superoleophobic surfaces were deemed to be superhydrophobic. However, recently, surfaces that are superoleophobic and yet superhydrophilic have also been reported [55]. In order to distinguish these counter-intuitive surfaces, these surfaces are known as superomniphobic surfaces. These surfaces are known to possess both superhydrophobicity and superoleophobicity [56, 57].

2. Design and development of superomniphobic surfaces

Superomniphobic surfaces show high contact angles and low contact angle hysteresis for virtually all liquids, including low surface tension liquids. In this section, the importance of roughness and re-entrant texture of a surface in obtaining high contact angles and low contact angle hysteresis with low surface tension liquids has first been discussed. Subsequently, the importance of hierarchically structured surfaces in further increasing the contact angles and decreasing the contact angle hysteresis [54] has been discussed.

The primary measure of wetting of a liquid on a non-textured (or smooth) surface is the equilibrium contact angle θ , given by Young's relation [58]:

$$\cos \theta = \frac{\gamma_{sv} - \gamma_{sl}}{\gamma_{lv}} \quad (1)$$

where, θ is Young's contact angle, γ_{sv} is surface tension between solid phase and vapour phase, γ_{sl} between solid phase and liquid phase and γ_{lv} between liquid solid phase.

The Young's equation (1) is only valid for a flat and homogeneous surface with Young's contact angle smaller than 120°. When surfaces are not considered ideally smooth, rigid or chemically homogeneous, Young's models cannot be employed [59]. When a droplet of liquid contacts a textured substrate, it can adopt one of the following two configurations to minimize its overall free energy [51, 52, 60], the Wenzel [61] state or the Cassie–Baxter [62] state. In the Wenzel state, as shown in Fig. 2a, the contacting liquid droplet completely permeates the surface protrusions, forming the so-called "fully-wetted" interface. In this state, the apparent contact angle θ^* (i.e., the contact angle on a textured surface) is calculated using the Wenzel relation: [61]

$$\cos \theta^* = r \cos \theta \dots \dots \dots (2)$$

Here, r is the average surface roughness, defined as the ratio of the actual surface area to the projected surface area. Since r is always greater than unity, roughness amplifies both the wetting and nonwetting behavior of materials in the Wenzel state. In other words, $\cos \theta^* \gg 0$ if $\cos \theta > 0$ and $\cos \theta^* \ll 0$ if $\cos \theta < 0$. It should be noted that a droplet may not show the apparent contact angle described by Equation 2 due to contact line pinning at numerous surface asperities, which in turn increases the contact angle hysteresis [40, 63].

On the other hand, in the Cassie–Baxter state, as shown in Fig. 2b, the liquid does not completely wet the surface texture. Instead, pockets of air remain trapped underneath the liquid droplet. The liquid penetrates into the surface texture until the local texture angle (ψ) becomes equal to the equilibrium contact angle θ (expressed by Young's relation) for the three-phase contact line [48]. Consequently, substrates possessing re-entrant surface texture (i.e., texture angle $\psi < 90^\circ$) can support a composite (solid-liquid-air) interface even for low surface tension liquids, such as oils and alcohols, which show Young's contact angles $\theta < 90^\circ$ (Fig. 2b). The apparent contact angles in this state are typically calculated using Cassie–Baxter relation as:

$$\cos \theta^* = f_{sL} \cos \theta + f_{LV} \cos \pi = f_{sL} \cos \theta - f_{LV} \dots \dots \dots (3)$$

Here, f_{sL} is the area fraction of the solid-liquid interface, and f_{LV} is the area fraction of the liquid-air interface underneath the liquid droplet on a homogeneous surface. Note that for nonhomogeneous surfaces, f_{sL} and f_{LV} represent the local areal fractions of the solid-liquid

interface and the liquid-air interface, respectively, in the vicinity of three phases (solid-liquid and vapor) contact line.

In contrast to the Wenzel state, high values of f_{LV} in the Cassie–Baxter state promote high apparent contact angles and low contact angle hysteresis even for low surface tension liquids [48, 64]. Consequently, substrates with re-entrant surface texture that can lead to the formation of the Cassie–Baxter state even with low surface tension liquids are critical for designing superomniphobic surfaces. Hierarchically structured surfaces such as the lotus leaf [65] possess more than one scale of texture (a finer length scale texture on an underlying coarser length scale texture; Fig. 2c–e). When a hierarchically structured surface supports a contacting liquid droplet in the Cassie–Baxter state at all length scales, the liquid droplet shows higher apparent contact angles compared to surfaces that possess a single scale of texture. This is because of the air trapped at both the coarser length scale, as well as the finer length scale (Fig. 2e). The apparent contact angles on a hierarchical surface can be calculated by recursively writing the Cassie–Baxter relation as [43, 66]:

$$\cos \theta_n^* = (1 - f_{LV,n}) \cos \theta_{n-1}^* - f_{LV,n} \dots \dots \dots (4)$$

Here, n can be 1, 2, 3 and so on is the number of length scales of texture f_{LV} , n is the area fraction of the liquid-air interface for the n th scale of texture, and θ_n^* and θ_{n-1}^* are the apparent contact angles on hierarchically structured surfaces with n scales of texture and $n-1$ scales of texture, respectively. From Equation 4, it is evident that θ_n^* increases as the number of scales of texture n increases. Hierarchically textured surfaces that support a contacting droplet in the Cassie-Baxter state also show a lower contact angle hysteresis compared to surfaces that possess a single scale of texture [67, 68]. Contact angle hysteresis is related to energy barriers that a liquid droplet must overcome during its movement along a solid surface and it characterises the resistance to the droplet movement [69]. Lower solid-liquid contact area leads to less contact line pinning (i.e., lower resistance to droplet movement) and lower contact angle hysteresis. Typically, hierarchically structured surfaces have a significantly lower solid-liquid contact area compared to surfaces that possess a single scale of texture (Fig. 2e). This can lead to significantly lower contact angle hysteresis [70]. In addition, theoretical analysis [52] has shown that surfaces with two scales of texture can enhance the stability of the Cassie–Baxter state by providing more locations with re-entrant texture where the composite interface can be stable. Recent work [71, 72] has also shown that the overall free energy increasingly favors the Cassie–Baxter state over the Wenzel state with an increasing number of scales of texture. For

all these reasons, hierarchically structured surfaces possessing re-entrant texture are ideal for developing superomniphobic surfaces [54].

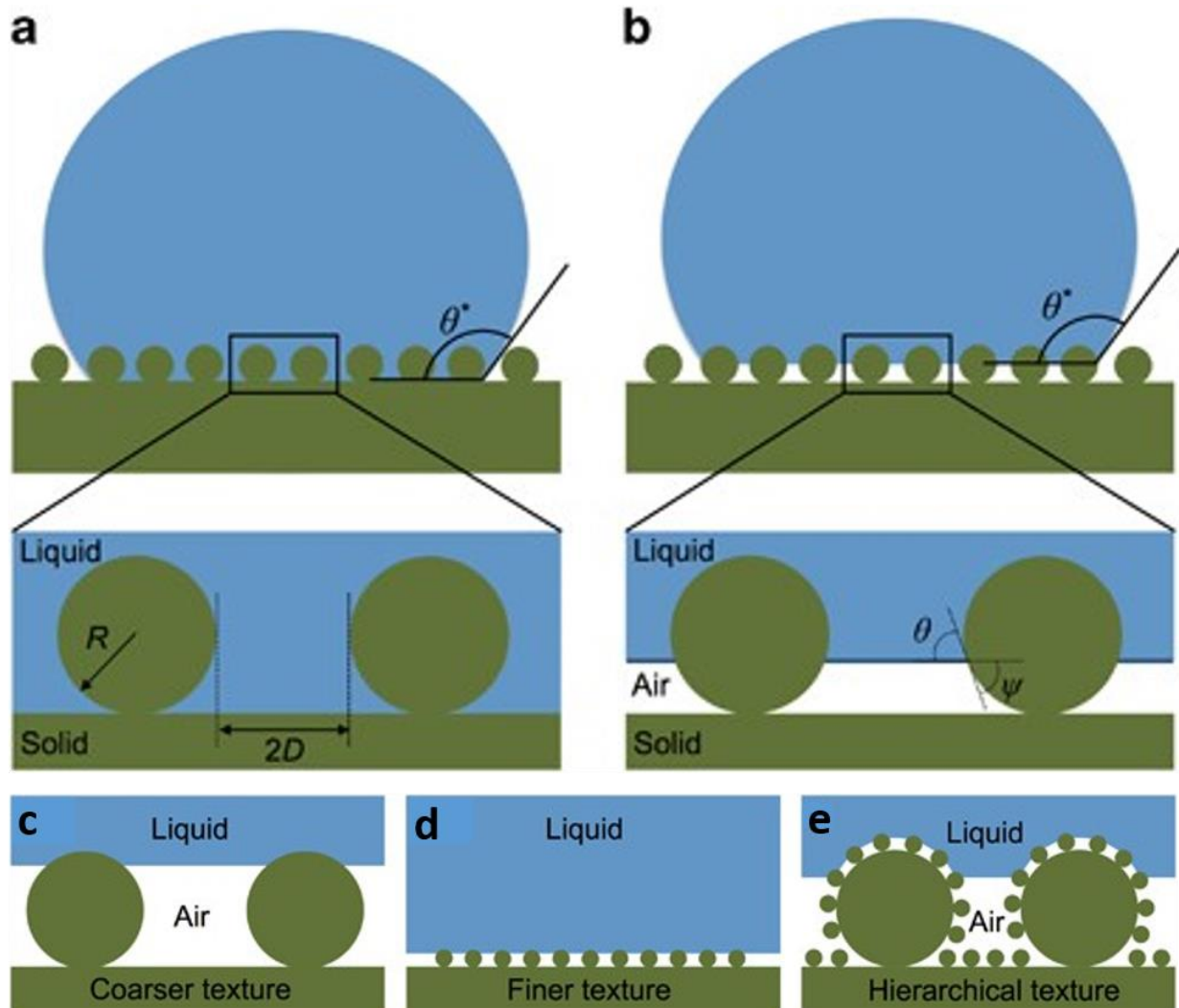


Fig.2 Liquid droplets on textured solid surfaces. (a, b) Schematic illustrations of a liquid droplet in the Wenzel state and the Cassie–Baxter state, respectively. In these schematics, R is the radius of the feature and $2D$ is the inter-feature spacing. Note that surfaces possessing re-entrant texture ($\psi < 90^\circ$) can support a robust composite (solid–liquid–air) interface even for low surface tension liquids that display $\theta < 90^\circ$, (c–e) Schematics of a liquid droplet in the Cassie–Baxter state on a coarser textured surface, a finer textured surface and a hierarchically textured surface, respectively [26]

Extant literature shows numerous research papers on superhydrophobic surfaces [16, 17, 73, 74]. Contrarily, there are very few papers on superoleophobic or superomniphobic surfaces. In this review article, the literature review was kept focused on fabrication of superomniphobic surfaces such as Nonfluorinated superomniphobic surfaces through polymeric micropillar arrays, Fabrication of superomniphobic coatings through layer-by-layer technique and an electrospun coating for the development of a superomniphobic surface etc.

2.1 Nonfluorinated superomniphobic surfaces through polymeric micropillar arrays

Kim et al. [1] developed a facile method to fabricate a flexible superomniphobic surface that can repel various liquids, including extremely low surface tension solvents. They fabricated doubly re-entrant mushroom-like micropillar (D-MP) structures using a conventional micro-molding technique to produce flat mushroom-like MP structures made of polydimethylsiloxane (PDMS) elastomer. Subsequently, metal thermal evaporation was performed on the surface. Due to the compressive residual stress of aluminum (Al) on the PDMS-based structures, the cap edges of the MPs became bent after the Al deposition, which led to the formation of D-MP structures on the surface. Generally, the superomniphobic surfaces are coated with perfluorocarbon materials to repel low surface tension liquids. However, despite the high surface energy of the Al layer and without the use of extra chemical treatments, the developed surfaces showed extreme liquid repellency with only the use of a microscale structure. The developed superomniphobic surface with D-MP structures not only exhibit extreme liquid repellency with a high liquid contact angle ($CA > 150^\circ$) and low sliding angle (SA) against a diverse range of liquid droplets but also maintained its super-repellency under a high strain ($\sim 50\%$), repeated cyclic stretching (>1000 cycles) even after oxygen plasma treatment. Also, viscous liquids such as blood could be repelled on the superomniphobic surface, even in a highly curved state. Moreover, the superomniphobic surfaces can be used in practical applications such as self-cleaning clothes and gloves [1, 75].

In a recent study (see Fig. 3a-(i)) an image of a springtail, and the corresponding scanning electron microscopy (SEM) images showed the regular texture on the skin. The SEM images showed the arrayed pillar structures with cavities with microscale diameter to cover the whole body of the insect. Fig. 3a-(ii) shows a schematic image of the skin of the springtail. Notably, the pillar structures on their skin featured mushroom-like doubly re-entrant structures in the cross-sectional view. These structures can suspend diverse liquids because the liquids become pinned under the downward edges of the cap, creating an air pocket between the surface and the liquid. Accordingly, springtails can breathe and survive in watery or oily environments.

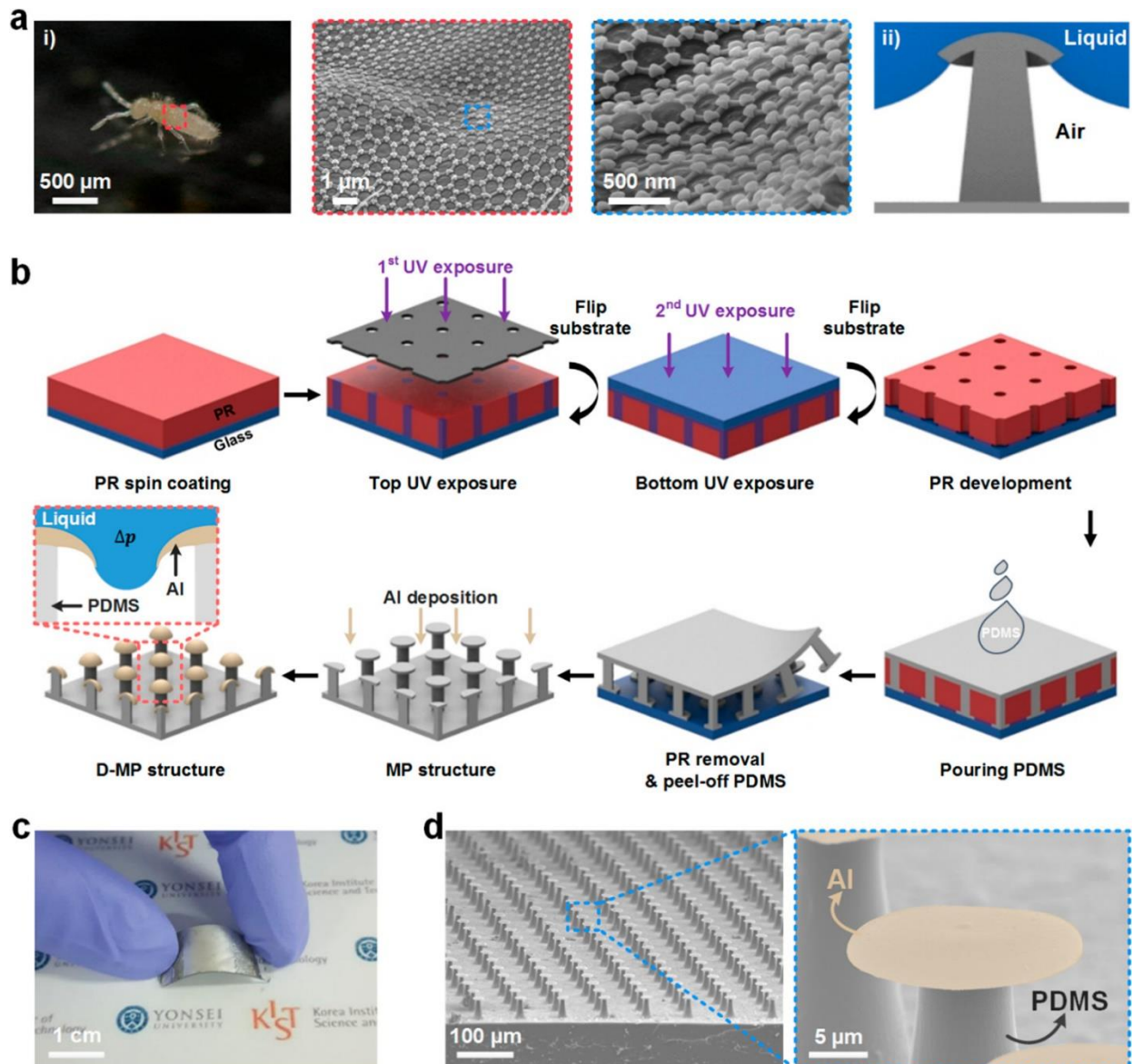


Fig 3. Fabrication of a D–MP structure as a flexible and nonfluorinated superomniphobic surface. (a-i) Photograph of a springtail and SEM images of the regular texture in the skin. (a-ii) A profile image of liquid suspension on the skin of the springtail. (b) Schematic diagram of the fabrication process of the D–MP structure. The inset shows a profile image of liquid suspension on the D–MP structure. (c) A photograph of the flexible and nonfluorinated D–MP patterned surface. (d) Low and high magnification SEM images of a D–MP array (cap diameter: 23 μm and Al overcoat: 50 nm) [1]

Fig. 3b shows the fabrication process of the D–MP structures on the PDMS substrate, mimicking special structures on the skin of springtails. Firstly, ultraviolet (UV) exposure with a photomask was conducted on top of the glass substrate covered with a photoresist to make the cavities of the micropillar structure. Subsequently, additional UV exposure without a photomask was conducted on the downside of the glass substrate. Since UV light can pass through glass substrates, only the thin bottom layer gets exposed to the UV light. During the development process, the UV exposed photoresist was removed from the top of the micropillars. When the developer reached the bottom layer, passing but limitedly through the micropillars, the thin

bottom layer exposed to UV light gets gradually removed, forming cavities like those observed in a mushroom cap structure. Through exact time control of the development process, the size of the bottom cavities could be adjusted. After pouring and curing the PDMS elastomer onto the developed photoresist mould, the entire photoresist was removed with ethanol, and the MP structures were obtained without any physical damage. Subsequently, Al was deposited on the MP structures to bend the cap edges of the MPs. Since the Al overcoat on the PDMS-based MP structures produces compressive residual stress, the cap edges of the MP structures permanently bent toward the polymer, forming D-MP structures. In this study, PDMS elastomer was chosen due to its adequate Young's modulus (≈ 3.5 MPa) for elastic deformation of the substrate itself and its ability to create D-MP structures after only nanometer-scale Al deposition onto the elastomer. The straightforward fabrication method is advantageous for the facile fabrication of D-MP patterned flexible superomniphobic surfaces that have high structural fidelity and uniformity, as shown in Fig. 3c and d.

To evaluate the wetting properties of MP and D-MP structures, researchers first compared the liquid repellency of the MP structure with that of the D-MP structure. The only structural difference between the MP structure and the D-MP structure was the presence or absence of downward facing cap edges. Fig. 4a shows optical images of deionized (DI) water (surface tension: 72 mN/m) and 50% ethanol solution (surface tension: ~ 28 mN/m) on the MP and D-MP structures [66, 67]. Even though both structures maintained super-repellency against DI water, the MP structure was fully wetted by the ethanol solution, but the D-MP structure still maintained super-repellency against the ethanol solution. This difference can be explained by the wetting mechanisms of both structures. Fig. 4b shows different wetting mechanisms of the MP and the D-MP structures. As the MP structure was made using a PDMS elastomer with a low surface energy (25 mN/m), DI water can form a CA (θ_i) larger than the cap edge angle (θ_{cap}) under the cap structure. Accordingly, a contact line between the DI water and the MP structure can be formed under the cap structure and the MP structure can suspend DI water in a super-repellent state.

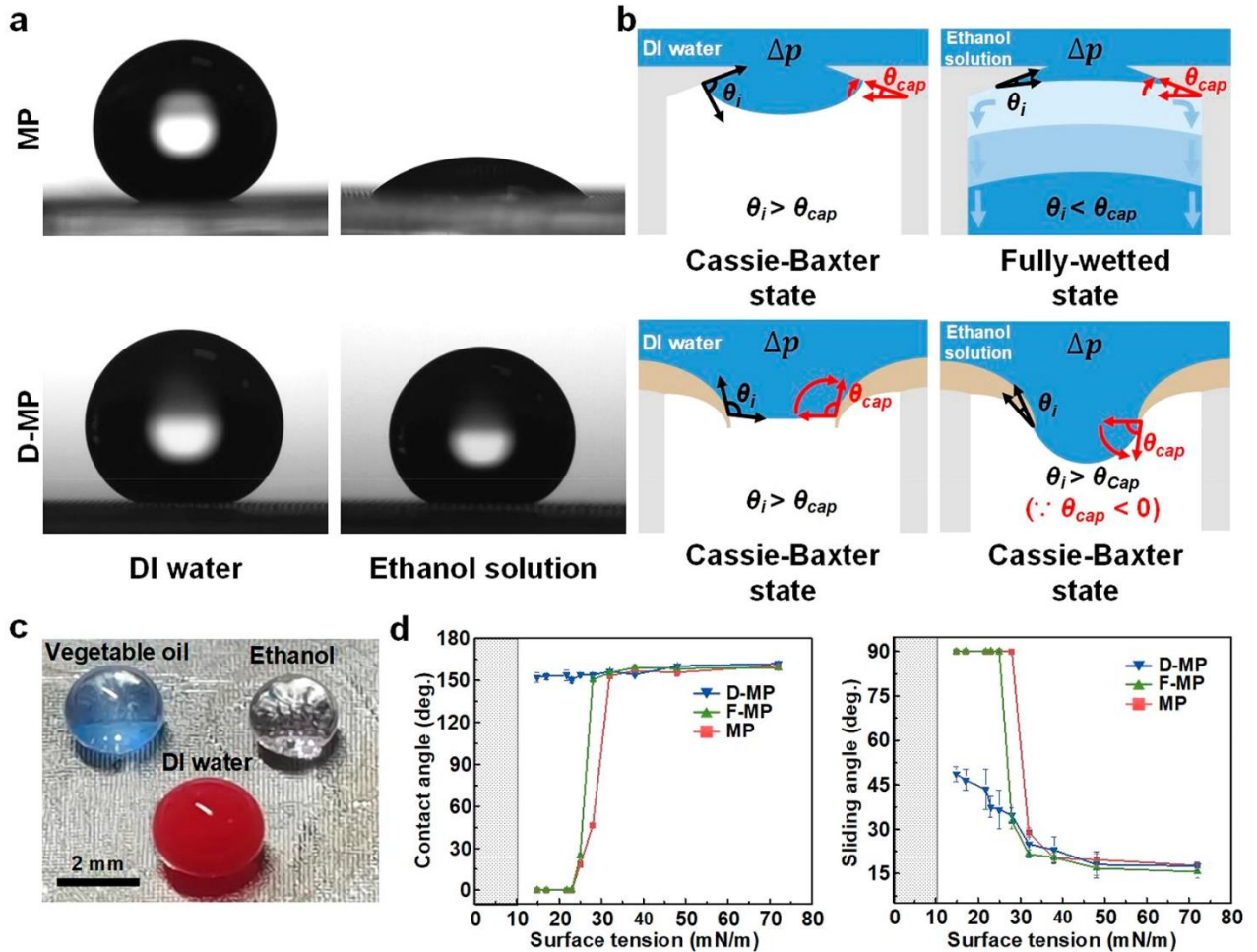


Fig. 4 Superomniphobicity of the D-MP structure. (a) Optical images of the DI water and ethanol solution droplets with a volume of 2 μL on the MP and D-MP structures. (b) Schematic images of different wetting mechanisms of the MP and D-MP structures. Δp is the pressure difference between the liquid and the air. (c) Photograph of DI water (red), vegetable oil (sky blue), and ethanol (transparent) droplets on the D-MP patterned surface. (d) The CAs and SAs of various liquid droplets on the MP, F-MP, and D-MP structures (the patterned box indicates that no liquids were available below 10 mN/m) [1]

However, it cannot form a contact line between ethanol solution and the MP structure under the cap structure due to the low surface tension of the liquid ($\theta_i < \theta_{cap}$). Thus, the ethanol solution pushes into the cavities and fully wets the MP structure. Different from the MP structure, the D-MP structure also exhibits super-repellency against the ethanol solution. This is because the downward facing cap edges of the D-MP structure form a negative cap edge angle ($\theta_{cap} < 0^\circ$) where the liquid moves upward to wet the whole structure. Therefore, a contact line between the ethanol solution and the D-MP structure gets formed under the downward cap edges despite the low surface tension of the liquid. In this context, even extremely low-surface-tension liquids ($\theta_i < 10^\circ$) can form a contact line under the downward cap edges of the D-MP structure. Fig. 4c shows the super-repellency behavior against a diverse range of liquids such as DI water, vegetable oil (surface tension: 32 mN/m), and ethanol (surface tension: 21.8

mN/m) on the D–MP structure-patterned surface. To quantify the liquid repellency of the MP and D–MP structures, researchers have measured the CAs and SAs of a diverse range of liquids (Fig. 4d). Although the MP structure could not repel liquids with surface tensions below ~ 32 mN/m, the D–MP structure repelled all liquids, even including fluorinated solvents (Krytox 100; surface tension: 17 mN/m, FC-770; surface tension: 14.8 mN/m), maintaining large CAs ($>150^\circ$) without any chemical treatments. Given that even the perfluorocarbon-material-coated–MP (F–MP) structure is easily wetted by liquids with surface tensions below ~ 25 mN/m, the D–MP structure has extremely high resistance against liquids without requiring any chemical treatment. In addition to quantifying the CAs of liquids on the structure patterned surfaces, researchers also measured the CAs of liquids on nonpatterned flat surfaces to compare the measured θ_i values with the θ^* values. Notably, FC-770, a fluorinated solvent, formed an extremely low CA on the Al-flat PDMS surface ($\theta_i \approx 0^\circ$), while FC-770 existed in a super-repellent state ($\theta^* = 152.2^\circ$) on the D–MP structure. This difference can be explained by the fact that Al has much higher surface energy than that of FC-770, which leads to complete wetting of the Al-flat surface.

However, in the case of the D–MP patterned surface, its structure prevents the ingress of liquid into the cavities regardless of the intrinsically high surface energy of the Al and extremely low surface tension of the liquid. Generally, the size of liquid droplet influence their wetting state on a super-repellent surface because smaller liquid droplets exert a Laplace pressure higher than that of larger droplets [66-70]. To evaluate the resistance of the D–MP structure against the pressure exerted by the liquid, they dispensed a ~ 2 μL ethanol droplet, as an example of one of the volatile liquids, and observed the evaporation of the droplet on the surface. During the evaporation process, the exerted pressure can be calculated using the Young–Laplace equation, which can be expressed as:

$$\Delta p = 2 / \gamma R \quad (5)$$

where Δp is the pressure difference between the liquid and the air, γ is the surface tension of the liquid, and R is the droplet radius. As R reduces through evaporation (with a corresponding Δp value), the ethanol perfectly wetted the surface because of the high increase in the pressure exerted by the small droplet. This result showed that the D–MP structure can resist the pressure exerted by the droplet and maintain super-repellency when there is a reduction in the size of the droplet) [1, 24, 25, 76].

2.2 Fabrication of superomniphobic coatings through layer-by-layer technique

Philip et al. [77] developed a superomniphobic surface using a layer-by-layer technique, which was combined with the vapour deposition of a fluorosilane to create a novel fabrication method resulting in a durable, super-repellent coating. Such a coating comprises of four layers, deposited separately, each of which aids in the creation of a mechanically durable, superomniphobic coating. The technique builds on the approach previously reported for superoleophobic/superhydrophilic coatings [78], which utilises charged layers using a layer-by-layer technique. Through the addition of an uncharged layer on top of the layer-by-layer stack, it is possible to achieve superomniphobicity. Fig. 5a shows the final coating composition and the chemical structure of the individual components of this novel combination of techniques. Polydiallyldimethylammonium chloride (PDDA) was chosen as the polymer base layer as it has a high cationic charge density and has been shown to bind strongly to glass substrates [78] and SiO₂ nanoparticles. The specific molecular weight range (100,000–200,000) was chosen to balance mechanical properties and ease of deposition (viscosity). Untreated, hydrophilic SiO₂ nanoparticles were used to enhance the roughness of coating. The negatively charged surface silanol groups ensured favorable interactions with the positively charged polymer layers. Additionally, SiO₂ nanoparticles are known to have high hardness [79] and wear resistance [79], which aided the fabrication of a mechanically durable coating [80]. Particles of 7 nm diameter were selected with the goal of creating a transparent coating. The fluorosilane (FL) was selected to provide repellency because of its low surface tension fluorinated tail and ability to form a self-assembled layer via vapor phase deposition.

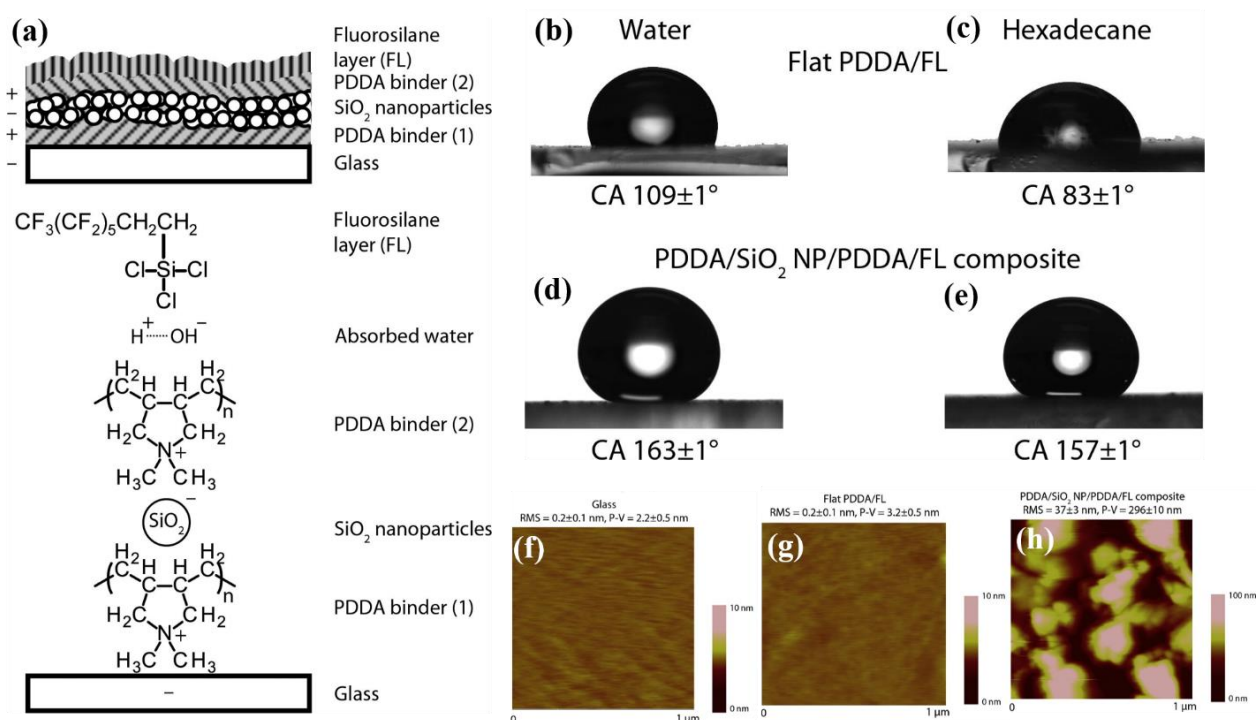


Fig. 5 (a) Schematic of layer-by-layer composite coating. Each layer is deposited separately. Also shown are the chemical composition and charge of each layer. The fluorosilane (FL) condenses onto the layer-by-layer stack via absorbed water; **(b-e)** Hexadecane and water droplets (5 μL) deposited on a flat and layer-by-layer composite coating with SiO_2 NP concentration of 15 mg mL^{-1} ; **(f-h)** AFM surface height maps with RMS and P–V roughness value for glass, PDDA/FL, and layer-by-layer composite coating with SiO_2 NP concentration of 15 mg mL^{-1} [77].

Initially, two layers were spray coated with PDDA (52 mg mL^{-1} , thickness ca. 200 nm) followed by a vapor deposited FL (PDDA/FL) on glass substrates to determine the oil-repellency of the flat polyelectrolyte–fluorosilane coating.

Fig. 5 (b-e) shows schematic pictures of the contact angles for droplets of water and hexadecane deposited on this coating. Table 1 provides a summary of all contact angle data. The flat coating was found to result in finite contact angles for all liquids tested, in contrast to bare glass and PDDA coatings, which were wetted by all the liquids (contact angle $< 5^\circ$). The PDDA/FL coating repels oils to some extent (finite contact angles) in addition to being hydrophobic with a water contact angle of $109 \pm 1^\circ$. To enhance the repellency, roughness was introduced via spray deposition of a SiO_2 nanoparticle layer (15 mg mL^{-1}).

Fig. 5 (f-h) shows the AFM surface height maps, RMS and P–V values determined from several $1 \times 1 \mu\text{m}^2$ scan areas of the various surfaces. These measurements confirmed the increase in contact angles of water and oil due to the formation of a composite air/solid interface typically known as the Cassie–Baxter state.

Table 1: Comparison of various liquids deposited on flat (PDDA/FL) and layer-by-layer composite coatings [81]

Liquid	Surface tension (mN m^{-1})	Flat PDDA/FL coating	Layer-by-layer composite coating	
		Contact angle ($^\circ$)	Contact angle ($^\circ$)	Tilt angle ($^\circ$)
Octane	21.14	62 ± 2	155 ± 1	9 ± 1
Decane	23.37	69 ± 2	159 ± 1	7 ± 1
Dodecane	25.35	76 ± 1	159 ± 1	5 ± 1
Tetradecane	26.13	78 ± 1	158 ± 1	4 ± 1
Hexadecane	27.05	83 ± 1	157 ± 1	4 ± 1
Water	71.99	109 ± 1	163 ± 1	2 ± 1

2.3 An electrospun coating for the development of a superomniphobic surface

Hierarchically structured surfaces possess more than one scale of texture (a finer length scale texture on an underlying coarser length scale texture). When a hierarchically structured surface

supports a contacting liquid droplet in the so-called Cassie–Baxter state [62] the liquid droplet shows high apparent contact angles and low contact angle hysteresis [3, 82–84]. Previous works [43–48, 51, 53, 85, 86] have explained the significance of reentrant curvature in designing surfaces that can support low surface tension liquids in the Cassie–Baxter state. Consequently, hierarchically structured surfaces possessing re-entrant curvature are expected to be very useful in developing surfaces that are extremely repellent to low surface tension liquids [97]. In this manner, Shuaijun et al. [70], employed an electrospun coating of cross-linked poly(dimethylsiloxane) (PDMS) + 50 wt% fluorodecyl polyhedral oligomeric silsesquioxane (POSS) (solid surface energy, $\gamma_{sv} \approx 11.5$ mN/m; on top of stainless steel wire meshes to fabricate hierarchically structured surfaces (Fig. 6a). PDMS was chosen in this work since cross linking enables this material system to possess excellent chemical resistance against a range of different chemicals. The low solid surface energy of the cross-linked PDMS + 50 wt% fluorodecyl POSS blends is due to the preferential segregation of fluorodecyl POSS ($\gamma_{sv} \approx 10$ mN/m) molecules on to the surface [45] (Fig. 6b). The hierarchically structured surfaces they developed possess re-entrant curvature at the coarser length scales (Fig. 6aA) as well as the finer length scale (Fig. 6c). The hierarchical texture (spacing ratio [70] $D^*_{\text{particle}} = 12.7$ and $D^*_{\text{fiber}} = 1.7$) along with the re-entrant curvature and the low surface energy of the coating results in high apparent contact angles (Fig. 6e) for a range of different polar and nonpolar low surface tension Newtonian liquids, including various acids, bases and solvents. Further, the surfaces possess low contact angle hysteresis and low roll-off angles $\omega \leq 2^\circ$ (Fig. 6d) for essentially all Newtonian liquids. There have been very few papers on surfaces showing such low contact angle hysteresis and low roll-off angles with extremely low surface tension liquids $\gamma_{lv} < 25$ mN/m. These surfaces possess low contact angle hysteresis and low roll-off angles because of the hierarchical structure with re-entrant curvature. The experimentally measured roll-off angles match reasonably well with the predictions based on the work by Furnidge [97]. Due to the low contact angle hysteresis, even jets of a range of different Newtonian liquids easily bounce on hierarchically structured surfaces (shown earlier in Fig. 6f). The hierarchically developed structured surfaces show exceptional chemical resistance as they can cause virtually all organic and inorganic Newtonian liquids to bounce and roll off [70].

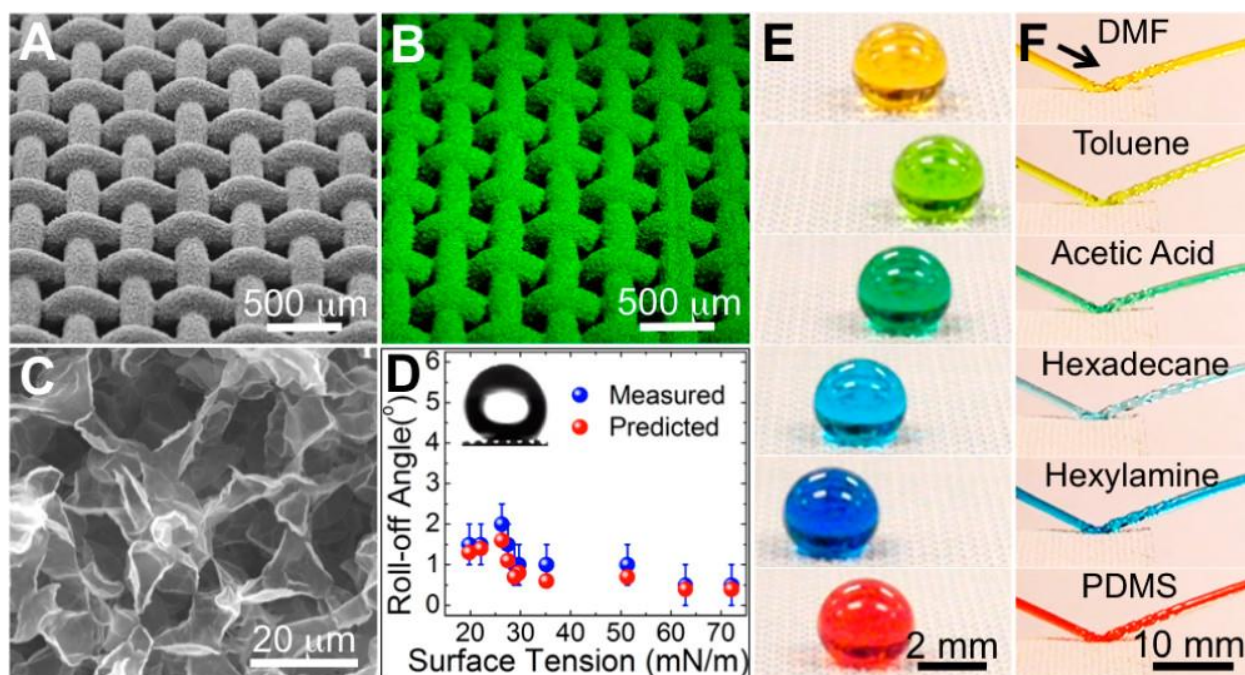


Fig. 6 (A) SEM image of the hierarchically structured surface illustrating the electrospun coating of cross-linked PDMS + 50 wt% fluorodecyl POSS on a stainless steel wire mesh 70. (B) Elemental mapping of fluorine on the hierarchically structured surface. The high surface fluorine content is expected to be due to the surface migration of the fluorodecyl POSS molecules. (C) SEM image illustrating the re-entrant curvature of the electrospun texture. (D) Roll-off angles for various Newtonian liquids on the surface shown in (A). The inset shows an ethanol droplet rolling on the surface at a roll-off angle $\omega = 2^\circ$. (E) Droplets of various low surface tension Newtonian liquids showing very high contact angles on the surface shown in (A). (F) Jets of different Newtonian liquids shown in (E) bouncing on the surface shown in (A) [70]

In this manner, a wide range of materials from metals to polymers and a wide range of surface coatings from perfluoralkyl silanes to fluorinated precursors have been used for the fabrication of superomniphobic surfaces. Hsieh et al. [87] fabricated stacks of silica spheres with a two-tier hierarchical texture using a two-stage spin-coating technique (Fig. 7a–c). When the surfaces were subsequently spin-coated with a perfluoroalkyl methacrylic copolymer, they showed $\theta^*_{adv} \approx 150^\circ$ and $\Delta\theta^* \approx 3^\circ$ for hexadecane. They also measured the contact angle hysteresis for a wide variety of liquids (Fig. 7d) with surface tension values γ_{LV} varying between 23.4 and 72.1 mN m⁻¹. They reported that the contact angle hysteresis increased with decreasing γ_{LV} on the surfaces. Daramanin et al. [87] electrochemically deposited spherical nanoporous films of poly(3,4-ethylenedioxyppyrole) on textured micropillar surfaces fabricated using photolithography. These substrates showed $\theta^*_{adv} = 153^\circ$, $\Delta\theta^* = 35^\circ$ and $\alpha = 27^\circ$ with 6 μ l hexadecane droplets. However, the same surface showed much higher contact angles with 6 μ l sunflower oil droplets ($\gamma_{LV} = 31$ mN m⁻¹, $\theta^*_{adv} = 155^\circ$, $\Delta\theta^* = 4^\circ$ and $\alpha = 3^\circ$).

Yang et al. [88] fabricated aluminum sheets with a hierarchical structure composed of distorted nanoscale flakes on microscale protrusions (Fig. 7e and 7f). Although the microscale

protrusions and pores were obtained by etching with hydrochloric acid, the nanoscale flakes were obtained by dipping the etched structure in boiling water. Upon modifying the surface with perfluorooctanoic acid, the surface showed $\theta^*=158^\circ$, 156° , 155° and 152° , $\Delta\theta^*=5^\circ$, 8° , 18° and 45° and $\alpha=5^\circ$, 7° , 15° and 40° with $\sim 5 \mu\text{l}$ droplets of rapeseed oil, hexadecane, dodecane ($\gamma_{LV}=25.3 \text{ mN m}^{-1}$) and decane ($\gamma_{LV}=23.8 \text{ mN m}^{-1}$), respectively, as shown in Fig. 7g. In the subsequent work, Yang et al. [82] fabricated hierarchical structures by spray coating a suspension of copper perfluorooctanoate in ethanol (Fig. 7h and 7i). The spray-coated surfaces showed $\theta^*=155^\circ$ and 156° and $\alpha=15^\circ$ and 40° with $\sim 8 \mu\text{l}$ droplets of rapeseed oil and hexadecane, respectively (Fig. 7j). The fabricated surface floats on a bath of hexadecane, as hexadecane cannot penetrate the surface texture (Fig. 7k) [26].

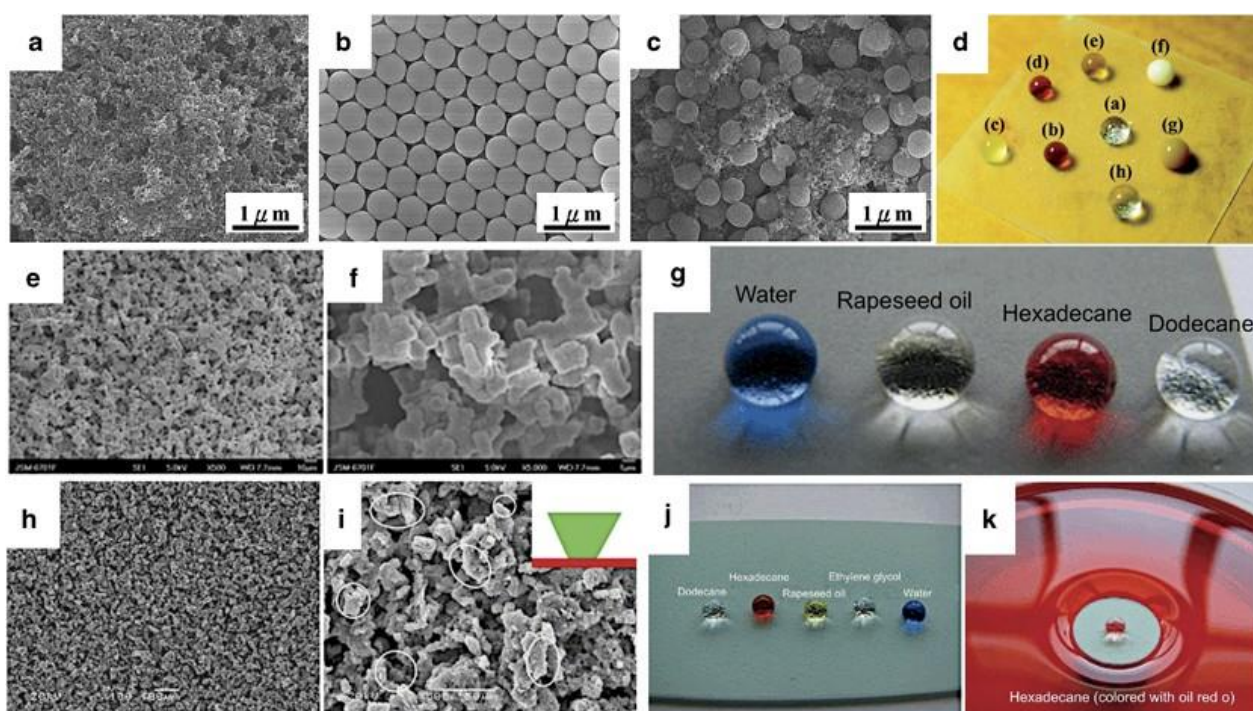


Fig. 7 Superomniphobic surfaces with hierarchical structure. (a–c) SEM images of stacks of silica spheres with finer texture, coarser texture and hierarchical texture, respectively. (d) A wide variety of liquid droplets display very high apparent contact angles and low contact angle hysteresis on a hierarchically textured surface coated with a perfluoroalkyl methacrylic copolymer. (e) An SEM image of microstructures with large numbers of protrusions and pores on the aluminum surface. (f) Magnified SEM image showing Nanoflakes that cover these microstructures. (g) A variety of liquid droplets displaying very high contact angles on the corresponding superomniphobic surface. (h–i) SEM images showing a hierarchically textured surface spray-coated with copper perfluorooctanoate at low and high magnifications, respectively. (j) A variety of liquid droplets displaying very high contact angles on the corresponding superomniphobic surface. (k) The spray-coated substrate shown in panel (h) floats on a bath of hexadecane, indicating the high hexadecane repellency of the spray-coated surface. [26]

4. Applications of superomniphobic surfaces

The durability of superomniphobic surfaces must be improved before they can be used in commercial applications, including self-cleaning, non-fouling, stain-free clothing and spill-

resistant protective wear and drag reduction. Apart from these applications, a few new niche applications of superomniphobic surfaces have started to emerge in the past few years. Some of these applications are discussed next.

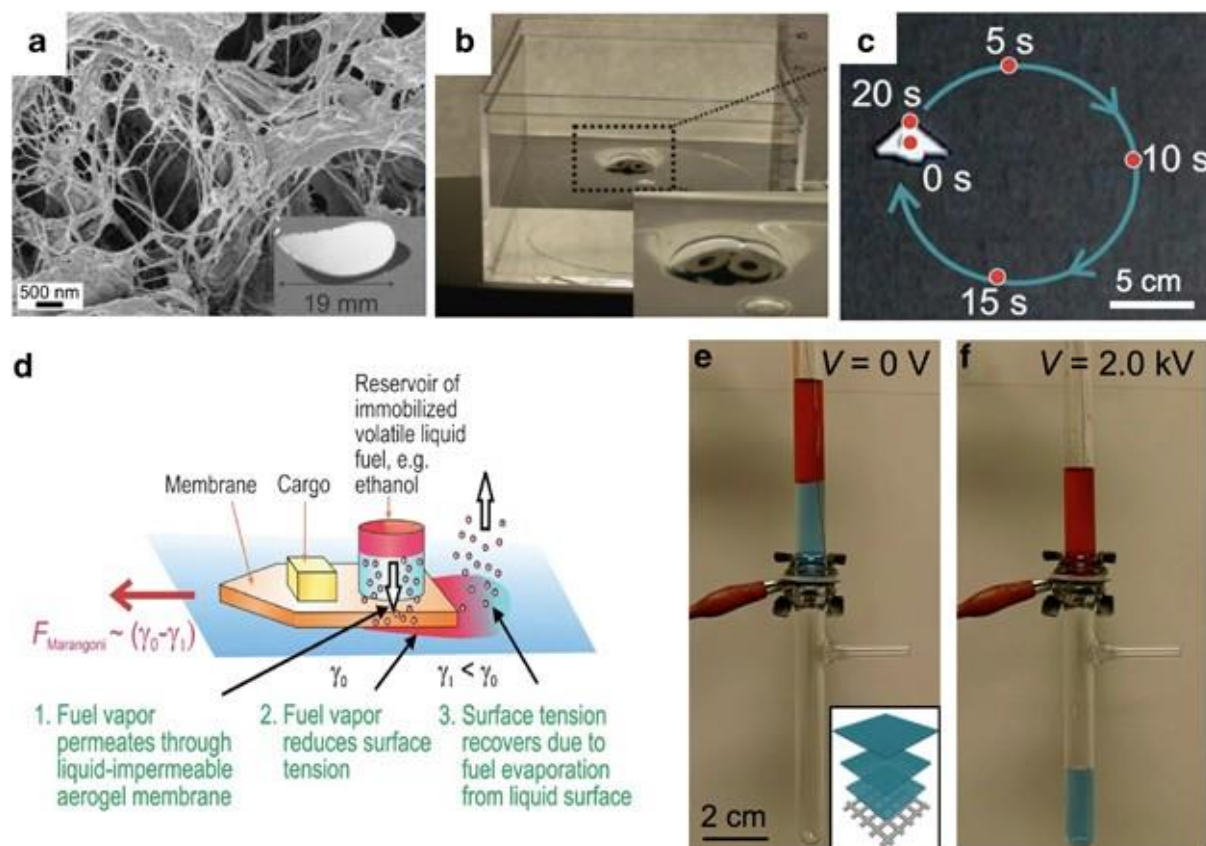


Fig 8. Applications of superomniphobic surfaces. (a) An s.e.m. image of nanocellulose aerogel with highly porous structure. Inset shows a superomniphobic nanocellulose aerogel membrane. (b) Superomniphobic aerogel membrane floats on water (and on various oils) and can carry a weight nearly three orders of magnitude larger than the weight of the aerogel itself. (c) Superomniphobic aerogel membrane traveling in circular trajectories at steady velocity. (d) A cartoon illustrating self-propulsion of superomniphobic aerogel membrane driven by fuel vapor. (e) A superomniphobic membrane can support a liquid column before the application of an electric field. The inset shows a schematic of the membrane module. (f) Upon application of an electric field, water (blue) permeates through, while hexadecane (red) is retained above the membrane when a voltage $V=2.0 \text{ kV}$ is applied. This allows for the facile, on-demand separation of a range of different oil–water mixtures [26]

Jin et al. [13] developed ultra-lightweight superomniphobic aerogels (Fig. 8a) that can float on both high and low surface tension liquids. The superomniphobic aerogels were fabricated by treating nanocellulose-based aerogel membranes with perfluorinated trichlorosilane. Most significantly, the superomniphobic aerogels could carry weight nearly three orders of magnitude larger than the weight of the aerogel itself (Fig. 8b). Such extraordinary load-carrying capacities make these superomniphobic aerogels viable candidates for (a) microrobots that are used in marine reconnaissance operations, and (b) microrobots for environmental sensing in aqueous and chemical environments. In their subsequent work, Jin et al. [89]

imparted their superomniphobic aerogels with the ability to self-propel using vapor-driven marangoni convection (Fig. 8c and d). Arun et al., [26] developed superomniphobic membranes that can separate polar and non-polar liquid mixtures into almost pure constituents on-demand on being subjected to electric field. The superomniphobic membranes were fabricated by dip-coating interwoven nylon membranes with polymer–fluoroPOSS blends. As a consequence of electrowetting [90-92], a polar liquid droplet in the Cassie–Baxter state on a porous membrane can transition to the Wenzel state when an electric field is applied across the porous membrane [93, 94]. Typically, a non-polar liquid does not undergo such a transition. Consequently, on application of electric field, the polar liquid permeates through the membrane, while the non-polar liquid retains above the membrane. Utilizing this preferential wettability transition of polar liquids over non-polar liquids, they demonstrated on-demand separation of free oil and water, oil-in-water emulsions and water-in-oil emulsions, with X99.9% separation efficiency (Fig. 8e and f). Such separation based methods opens up new avenues for remote operation of oil–water separation units, microfluidic valves and lab-on-a-chip devices.

The performance goals listed in Table 2 can help material developers to design clothing materials to help minimize the risk of hypothermia for soldiers exposed to the cold/extreme cold environments, or heat stress in a hot and humid environment. Likewise, to improve the soldiers' survival when carrying out their mission in a contaminated battlefield, omniphobic coated clothing can repel and prevent toxic industrial chemicals (TICs) and warfare agents from wetting the clothing and from wetting through the protective clothing's barrier layer. Additionally, to extend the durability and longevity of the omniphobic coating, tests such as launderability, torsional flexibility and tensile strength can be performed. The omniphobic coating must also have minimal effects on the base textile material's physical properties such as air permeability, weight, thickness and dimensional stability. Since blending with the environment's background minimizes detection by the enemy force, camouflaging is critical for soldiers' survival on a battlefield; therefore, color fastness is very important, and the omniphobic coating must have minimal change to the clothing's dyed camouflaging patterns on its outer shell fabric [95-99].

Table 2: Performance goals for development of superomniphobic coated fabrics [100]

Performance	Tests and measurements	Test method	Performance goals	Test equipment
Liquid repellency performance	1. Surface tension 2. Apparent contact angle (CA) 3. Roll off CA 4. Timed droplet wetting	ASTM D5946 (water, oil and solvents), 20 μ L drop	18 dynes/cm/ Apparent CA > 150° Roll off CA < 5°	 Rame Hart Goniometer Model 300-00-115, with automatic tilt base
Thermal comfort	Sweating guarded hot plate	ASTM D1518	Compare to untreated fabric: Clo \leq 5% and I _m \leq 10%	 NSRDEC Sweating guarded hotplate test chamber
Durability	Abrasion resistance	ASTM D3884	\geq 2000 cycles. After abrasion, apparent CA \geq of base fabric	 Tabor Twin Abrader
Physical comfort	Dimensional stability	AATCC 135	< 3% for both W and F directions, after 1 and 5 launderings	 Launder-Ometer

5. Conclusions and future perspective

The development of superomniphobic surfaces is an area of significant academic and industrial interest due to the wide range of emerging applications. Multifunctional properties including anti-fouling (where superomniphobicity and nanostructuring are of importance, especially for anti-biofouling), self-cleaning, anti-smudge, low-drag applications will significantly be enabled by rapid advances in developing long lasting superomniphobic surfaces. This paper sheds deep insights on various design and manufacturing considerations necessary to fabricate multifunctional superomniphobic surfaces using various materials ranging from perfluoralkyl silanes to fluorinated precursors as well as fabrication techniques ranging from physical

methods to chemical methods. The broad conclusions of this review can be summarised as below:

- (i) A robust superomniphobic surface must qualify two principal conditions: (1) it must possess an appropriate low surface tension to form a contact angle $>150^\circ$ and contact angle hysteresis $<5^\circ$ both for oil and water (2) it should possess a sufficiently high breakthrough pressure to withstand the applied pressure from the contacting low surface tension liquid to prevent the transition from the Cassie–Baxter state to the Wenzel state.
- (ii) Five major factors were identified to influence the performance of superomniphobic surfaces which are (1) surface chemistry, (2) surface roughness, (3) Cassie and Baxter state, (4) re-entrant texture and (5) polarity of liquids and wetting surface.
- (iii) Attempts to fabricate nonfluorinated, flexible superomniphobic surface inspired by the structural features of the skin of springtails showed that super-repellency remained preserved even under high strain ($\sim 50\%$), repeated cyclic stretching, bending and twisting (>1000 cycles).
- (iv) An adapted layer-by-layer approach involving charged species with electrostatic interactions between layers was combined with an uncharged fluorosilane layer. This resulted in the development of a durable superomniphobic coating with water and hexadecane contact angles exceeding 155° and tilt angles of 4° or less. This coating fabricated with SiO_2 was mechanically durable and repellent to liquids with surface tensions ranging from 72 to 21 mN m^{-1} .
- (v) Newer advances reveal that superomniphobicity can be achieved using a wide range of different non-Newtonian liquids and Newtonian liquids. Such surfaces possess hierarchical scales of re-entrant texture that significantly reduce the solid–liquid contact area. Virtually all liquids including concentrated organic and inorganic acids, bases, and solvents, as well as viscoelastic polymer solutions, can easily roll off. Consequently, they can serve as effective chemical shield against all liquids whether organic or inorganic, polar or nonpolar, Newtonian or non-Newtonian.

One growth area for future research in this area would be incorporation of repellent coatings for textile applications in insect repellency. The effects of superomniphobic coatings on properties that are yet to be evaluated include thermal signature, spectral reflectance and static discharge for military applications. However, growing imperative in this area will lead to an exciting future in the synthesis of novel superomniphobic surfaces which will empower rapid

advances in healthcare, textile, aerospace, transport, composites and many other new emerging applications which have yet to harness the full potential of superomniphobic surfaces.

Acknowledgments

SG acknowledge the financial support provided by the UKRI via Grants No. EP/S036180/1, EP/T001100/1 and EP/T024607/1, feasibility study awards to LSBU from the UKRI National Interdisciplinary Circular Economy Hub (EP/V029746/1) and Transforming the Foundation Industries: a Network+ (EP/V026402/1), the Royal Academy of Engineering via Grant No. IAPP18-19\295, EURAMET EMPIR A185 (2018) from H2020 and Hubert Curien Alliance Award from the British Council.

References

1. Kim, H., et al., *Nonfluorinated superomniphobic surfaces through shape-tunable mushroom-like polymeric micropillar arrays*. ACS applied materials & interfaces, 2018. **11**(5): p. 5484-5491.
2. Verma, J., et al., *Irradiation effect of low-energy ion on polyurethane nanocoating containing metal oxide nanoparticles*. Radiation Effects and Defects in Solids, 2017. **172**(11-12): p. 964-974.
3. Sun, T., et al., *Bioinspired surfaces with special wettability*. Accounts of chemical research, 2005. **38**(8): p. 644-652.
4. Genzer, J. and K. Efimenko, *Recent developments in superhydrophobic surfaces and their relevance to marine fouling: a review*. Biofouling, 2006. **22**(5): p. 339-360.
5. Leng, B., et al., *Superoleophobic cotton textiles*. Langmuir, 2009. **25**(4): p. 2456-2460.
6. Lee, C. and C.-J. Kim, *Underwater restoration and retention of gases on superhydrophobic surfaces for drag reduction*. Physical review letters, 2011. **106**(1): p. 014502.
7. Golovin, K.B., et al., *Bioinspired surfaces for turbulent drag reduction*. Philosophical Transactions of the Royal Society A: Mathematical, Physical and Engineering Sciences, 2016. **374**(2073): p. 20160189.
8. Zhang, X., et al., *Bioinspired aquatic microrobot capable of walking on water surface like a water strider*. ACS applied materials & interfaces, 2011. **3**(7): p. 2630-2636.
9. Verma, J., A. Khanna, and A. Bhattacharya, *Anti-algal study on polymeric coating containing metal@ metal oxide core-shell nanoparticles developed through organic synthesis for marine paint applications*. Advances in Organic Synthesis: Volume 15, 2021. **5**: p. 98.
10. Verma, J., et al., *Super protective anti-bacterial coating development with silica–titania nano core–shells*. Nanoscale Advances, 2020. **2**(9): p. 4093-4105.
11. Verma, J. and A. Bhattacharya, *Development of coating formulation with silica–titania core–shell nanoparticles against pathogenic fungus*. Royal Society Open Science, 2018. **5**(8): p. 180633.
12. Verma, J., et al., *Development of polyurethane based anti-scratch and anti-algal coating formulation with silica-titania core-shell nanoparticles*. Vacuum, 2018. **153**: p. 24-34.
13. Jin, H., et al., *Superhydrophobic and superoleophobic nanocellulose aerogel membranes as bioinspired cargo carriers on water and oil*. Langmuir, 2011. **27**(5): p. 1930-1934.
14. Larrañaga-Altuna, M., et al., *Bactericidal surfaces: An emerging 21st-century ultra-precision manufacturing and materials puzzle*. Applied Physics Reviews, 2021. **8**(2): p. 021303.

15. Han, H., et al., *Single-droplet multiplex bioassay on a robust and stretchable extreme wetting substrate through vacuum-based droplet manipulation*. ACS nano, 2018. **12**(2): p. 932-941.
16. Verma, J., A. Gupta, and D. Kumar, *Steel protection by SiO₂/TiO₂ core-shell based hybrid nanocoating*. Progress in Organic Coatings, 2022. **163**: p. 106661.
17. Verma, J., D. Kumar, and B. Sikarwar, *Fabrication of highly efficient nano core-shell structure for the development of super-hydrophobic polymeric coating on mild steel*. Polymers and Polymer Composites, 2022. **30**: p. 09673911221087835.
18. Wu, Y., et al., *Bioinspired design of three-dimensional ordered tribrachia-post arrays with re-entrant geometry for omniphobic and slippery surfaces*. ACS nano, 2017. **11**(8): p. 8265-8272.
19. Hsieh, C.-T., F.-L. Wu, and W.-Y. Chen, *Superhydrophobicity and superoleophobicity from hierarchical silica sphere stacking layers*. Materials Chemistry and Physics, 2010. **121**(1-2): p. 14-21.
20. Kota, A.K., et al., *Hierarchically structured superoleophobic surfaces with ultralow contact angle hysteresis*. Advanced materials, 2012. **24**(43): p. 5838-5843.
21. Wong, W.S., et al., *Omnidirectional self-assembly of transparent superoleophobic nanotextures*. Acs Nano, 2017. **11**(1): p. 587-596.
22. Mazumder, P., et al., *Superomniphobic, transparent, and antireflection surfaces based on hierarchical nanostructures*. Nano letters, 2014. **14**(8): p. 4677-4681.
23. Wong, W.S., et al., *Ultra-durable and transparent self-cleaning surfaces by large-scale self-assembly of hierarchical interpenetrated polymer networks*. ACS applied materials & interfaces, 2016. **8**(21): p. 13615-13623.
24. Dufour, R., et al., *From micro to nano reentrant structures: hysteresis on superomniphobic surfaces*. Colloid and Polymer Science, 2013. **291**(2): p. 409-415.
25. Kang, S.M., et al., *Robust superomniphobic surfaces with mushroom-like micropillar arrays*. Soft Matter, 2012. **8**(33): p. 8563-8568.
26. Kota, A.K., G. Kwon, and A. Tuteja, *The design and applications of superomniphobic surfaces*. NPG Asia Materials, 2014. **6**(7): p. e109-e109.
27. Yong, J., et al., *Nepenthes inspired design of self-repairing omniphobic slippery liquid infused porous surface (SLIPS) by femtosecond laser direct writing*. Advanced Materials Interfaces, 2017. **4**(20): p. 1700552.
28. Arzt, E., et al., *Functional surface microstructures inspired by nature—From adhesion and wetting principles to sustainable new devices*. Progress in Materials Science, 2021. **120**: p. 100823.
29. Watson, G.S., et al., *Insect analogue to the lotus leaf: a planthopper wing membrane incorporating a low-adhesion, nonwetting, superhydrophobic, bactericidal, and biocompatible surface*. ACS applied materials & interfaces, 2017. **9**(28): p. 24381-24392.
30. Neinhuis, C. and W. Barthlott, *Characterization and distribution of water-repellent, self-cleaning plant surfaces*. Annals of botany, 1997. **79**(6): p. 667-677.
31. Koch, K., H.F. Bohn, and W. Barthlott, *Hierarchically sculptured plant surfaces and superhydrophobicity*. Langmuir, 2009. **25**(24): p. 14116-14120.
32. Hu, D.L., B. Chan, and J.W. Bush, *The hydrodynamics of water strider locomotion*. nature, 2003. **424**(6949): p. 663-666.
33. Hu, D.L. and J.W. Bush, *Meniscus-climbing insects*. Nature, 2005. **437**(7059): p. 733-736.
34. Gao, X. and L. Jiang, *Water-repellent legs of water striders*. nature, 2004. **432**(7013): p. 36-36.
35. Autumn, K., et al., *Adhesive force of a single gecko foot-hair*. Nature, 2000. **405**(6787): p. 681-685.
36. Parker, A.R. and C.R. Lawrence, *Water capture by a desert beetle*. Nature, 2001. **414**(6859): p. 33-34.
37. Wagner, T., C. Neinhuis, and W. Barthlott, *Wettability and contaminability of insect wings as a function of their surface sculptures*. Acta Zoologica, 1996. **77**(3): p. 213-225.

38. Genzer, J. and K. Efimenko, *Creating long-lived superhydrophobic polymer surfaces through mechanically assembled monolayers*. Science, 2000. **290**(5499): p. 2130-2133.
39. Bhushan, B. and Y.C. Jung, *Natural and biomimetic artificial surfaces for superhydrophobicity, self-cleaning, low adhesion, and drag reduction*. Progress in Materials Science, 2011. **56**(1): p. 1-108.
40. Chen, W., et al., *Ultrasuperhydrophobic and ultralyophobic surfaces: some comments and examples*. Langmuir, 1999. **15**(10): p. 3395-3399.
41. Lafuma, A. and D. Quéré, *Superhydrophobic states*. Nature materials, 2003. **2**(7): p. 457-460.
42. Helbig, R., et al., *Smart skin patterns protect springtails*. PloS one, 2011. **6**(9): p. e25105.
43. Choi, W., et al., *Fabrics with tunable oleophobicity*. Advanced Materials, 2009. **21**(21): p. 2190-2195.
44. Tuteja, A., et al., *Robust omniphobic surfaces*. Proceedings of the National Academy of Sciences, 2008. **105**(47): p. 18200-18205.
45. Tuteja, A., et al., *Designing superoleophobic surfaces*. Science, 2007. **318**(5856): p. 1618-1622.
46. Ahuja, A., et al., *Nanonails: A simple geometrical approach to electrically tunable superlyophobic surfaces*. Langmuir, 2008. **24**(1): p. 9-14.
47. Cao, L., et al., *Super water-and oil-repellent surfaces on intrinsically hydrophilic and oleophilic porous silicon films*. Langmuir, 2008. **24**(5): p. 1640-1643.
48. Marmur, A., *From hydrophilic to superhydrophobic: theoretical conditions for making high-contact-angle surfaces from low-contact-angle materials*. Langmuir, 2008. **24**(14): p. 7573-7579.
49. Coulson, S.R., et al., *Super-repellent composite fluoropolymer surfaces*. The Journal of Physical Chemistry B, 2000. **104**(37): p. 8836-8840.
50. Coulson, S., et al., *Ultralow surface energy plasma polymer films*. Chemistry of materials, 2000. **12**(7): p. 2031-2038.
51. Marmur, A., *Wetting on hydrophobic rough surfaces: to be heterogeneous or not to be?* Langmuir, 2003. **19**(20): p. 8343-8348.
52. Nosonovsky, M., *Multiscale roughness and stability of superhydrophobic biomimetic interfaces*. Langmuir, 2007. **23**(6): p. 3157-3161.
53. Herminghaus, S., *Roughness-induced non-wetting*. EPL (Europhysics Letters), 2000. **52**(2): p. 165.
54. Kota, A.K., W. Choi, and A. Tuteja, *Superomniphobic surfaces: Design and durability*. MRS bulletin, 2013. **38**(5): p. 383-390.
55. Liu, K., Y. Tian, and L. Jiang, *Bio-inspired superoleophobic and smart materials: design, fabrication, and application*. Progress in Materials Science, 2013. **58**(4): p. 503-564.
56. Kota, A.K., J.M. Mabry, and A. Tuteja, *Superoleophobic surfaces: design criteria and recent studies*. Surface Innovations, 2013. **1**(2): p. 71-83.
57. Kota, A.K., et al., *Hygro-responsive membranes for effective oil-water separation*. Nature communications, 2012. **3**(1): p. 1-8.
58. Young, T., III. *An essay on the cohesion of fluids*. Philosophical transactions of the royal society of London, 1805(95): p. 65-87.
59. Hawi, S., et al., *Critical review of nanopillar-Based mechanobactericidal systems*. ACS Applied Nano Materials, 2022. **5**(1): p. 1-17.
60. Johnson, R.E., *Contact angle, wettability, and adhesion*. Advances in chemistry series, 1964. **43**: p. 112.
61. Wenzel, R.N., *Resistance of solid surfaces to wetting by water*. Industrial & Engineering Chemistry, 1936. **28**(8): p. 988-994.
62. Cassie, A. and S. Baxter, *Wettability of porous surfaces*. Transactions of the Faraday society, 1944. **40**: p. 546-551.

63. Choi, W., et al., *A modified Cassie–Baxter relationship to explain contact angle hysteresis and anisotropy on non-wetting textured surfaces*. Journal of colloid and interface science, 2009. **339**(1): p. 208-216.
64. Callies, M. and D. Quéré, *On water repellency*. Soft matter, 2005. **1**(1): p. 55-61.
65. Richard, D. and D. Quéré, *Bouncing water drops*. EPL (Europhysics Letters), 2000. **50**(6): p. 769.
66. Herminghaus, S., *Roughness-induced non-wetting*. EPL (Europhysics Letters), 2007. **79**(5): p. 59901.
67. Bhushan, B., *Nanotribology and nanomechanics I–Measurement techniques, II–Nanotribology, biomimetics, and industrial applications, 3rd edn Springer*. 2011, Heidelberg.
68. Gao, L. and T.J. McCarthy, *The "lotus effect" explained: two reasons why two length scales of topography are important*. Langmuir, 2006. **22**(7): p. 2966-2967.
69. Johnson Jr, R.E. and R.H. Dettre, *Contact angle hysteresis. III. Study of an idealized heterogeneous surface*. The journal of physical chemistry, 1964. **68**(7): p. 1744-1750.
70. Pan, S., et al., *Superomniphobic surfaces for effective chemical shielding*. Journal of the American Chemical Society, 2013. **135**(2): p. 578-581.
71. Su, Y., et al., *Nano to micro structural hierarchy is crucial for stable superhydrophobic and water-repellent surfaces*. Langmuir, 2010. **26**(7): p. 4984-4989.
72. Bittoun, E. and A. Marmur, *The role of multiscale roughness in the lotus effect: is it essential for super-hydrophobicity?* Langmuir, 2012. **28**(39): p. 13933-13942.
73. Khaleque, T. and S. Goel, *Repurposing superhydrophobic surfaces into icephobic surfaces*. Materials Today: Proceedings, 2022.
74. Verma, J., et al., *Development of Hydrophobic Coating with Polymer–Metal Oxide Nanocomposites*, in *Advances in Industrial and Production Engineering*. 2019, Springer. p. 117-126.
75. Liu, T.L. and C.-J.C. Kim, *Turning a surface superrepellent even to completely wetting liquids*. Science, 2014. **346**(6213): p. 1096-1100.
76. Dufour, R., et al., *Engineering sticky superomniphobic surfaces on transparent and flexible PDMS substrate*. Langmuir, 2010. **26**(22): p. 17242-17247.
77. Brown, P.S. and B. Bhushan, *Mechanically durable, superomniphobic coatings prepared by layer-by-layer technique for self-cleaning and anti-smudge*. Journal of colloid and interface science, 2015. **456**: p. 210-218.
78. Brown, P.S. and B. Bhushan, *Mechanically durable, superoleophobic coatings prepared by layer-by-layer technique for anti-smudge and oil-water separation*. Scientific reports, 2015. **5**(1): p. 1-9.
79. Ebert, D. and B. Bhushan, *Durable Lotus-effect surfaces with hierarchical structure using micro- and nanosized hydrophobic silica particles*. Journal of colloid and interface science, 2012. **368**(1): p. 584-591.
80. Bhushan, B., *Introduction to tribology*. 2013: John Wiley & Sons.
81. Haynes, W., D. Lide, and T. Bruno, *Tetrabromobisphenol A*. CRC handbook of chemistry and physics, 2014: p. 3-158.
82. Bhushan, B. and Y.C. Jung, *Biomimetics inspired surfaces for superhydrophobicity, self-cleaning, low adhesion, and drag reduction*. Nanotribology and Nanomechanics II, 2011: p. 533-699.
83. Ma, M. and R.M. Hill, *Superhydrophobic surfaces*. Current opinion in colloid & interface science, 2006. **11**(4): p. 193-202.
84. Quéré, D., *Non-sticking drops*. Reports on Progress in Physics, 2005. **68**(11): p. 2495.
85. Lin, Y.-T. and J.-H. Chou, *Fabricating super-hydrophobic polydimethylsiloxane surfaces by a simple filler-dissolved process*. Japanese Journal of Applied Physics, 2010. **49**(12R): p. 127101.
86. Hoefnagels, H., et al., *Biomimetic superhydrophobic and highly oleophobic cotton textiles*. Langmuir, 2007. **23**(26): p. 13158-13163.

87. Hsieh, C.-T., F.-L. Wu, and W.-Y. Chen, *Contact angle hysteresis and work of adhesion of oil droplets on nanosphere stacking layers*. The Journal of Physical Chemistry C, 2009. **113**(31): p. 13683-13688.
88. Yang, J., et al., *Superoleophobic textured aluminum surfaces*. New Journal of Chemistry, 2011. **35**(11): p. 2422-2426.
89. Jin, H., et al., *Vapour-driven Marangoni propulsion: continuous, prolonged and tunable motion*. Chemical Science, 2012. **3**(8): p. 2526-2529.
90. Mugele, F. and J.-C. Baret, *Electrowetting: from basics to applications*. Journal of physics: condensed matter, 2005. **17**(28): p. R705.
91. Shamai, R., et al., *Water, electricity, and between... On electrowetting and its applications*. Soft Matter, 2008. **4**(1): p. 38-45.
92. Gras, S.L., et al., *Intelligent control of surface hydrophobicity*. ChemPhysChem, 2007. **8**(14): p. 2036-2050.
93. Manukyan, G., et al., *Electrical switching of wetting states on superhydrophobic surfaces: a route towards reversible Cassie-to-Wenzel transitions*. Physical review letters, 2011. **106**(1): p. 014501.
94. Oh, J., et al., *Electric-field-driven instabilities on superhydrophobic surfaces*. EPL (Europhysics Letters), 2011. **93**(5): p. 56001.
95. Hastbacka, M., *Non-fluorinated Omniphobic Coatings for Stain Resistant Textiles*. February 29, 2016.[5], 2016.
96. Zeng, C., et al., *Directional Water Transport Fabrics with Durable Ultra-High One-Way Transport Capacity*. Advanced Materials Interfaces, 2016. **3**(14): p. 1600036.
97. Moiz, A., *Application of superomniphobic finishes on fabrics for chemical protection*. 2018, RMIT University.
98. Bittner, R.W., K. Bica, and H. Hoffmann, *Fluorine-free, liquid-repellent surfaces made from ionic liquid-infused nanostructured silicon*. Monatshefte für Chemie-Chemical Monthly, 2017. **148**(1): p. 167-177.
99. Hensel, R., C. Neinhuis, and C. Werner, *The springtail cuticle as a blueprint for omniphobic surfaces*. Chemical Society Reviews, 2016. **45**(2): p. 323-341.
100. Truong, Q.T. and N. Pomerantz, *Military applications: Development of superomniphobic coatings, textiles and surfaces*, in *Waterproof and water repellent textiles and clothing*. 2018, Elsevier. p. 473-531.